

Joint Inversion of Receiver Function of Teleseismic Body Waves and Local Group Velocity Dispersion Curves beneath ESPZ and PMSA Stations (Antarctic Peninsula)

A. VUAN

Istituto Nazionale di Oceanografia e Geofisica Sperimentale, B.go Grotta Gigante 42/c,
34010 Sgonico (Trieste) - Italia (aless@ogs.trieste.it)

Received 26 January 2000, accepted in revised form 25 February 2001

Abstract - A database of 70 teleseismic earthquakes is used to infer the lithospheric structure beneath PMSA and ESPZ stations, deployed in Antarctic Peninsula respectively south of the intersection of the Hero Fracture Zone (HFZ) with the South Shetland Trench (SST), and at the extreme tip of the Antarctic Peninsula. The inversion of receiver function of teleseismic body waves is constrained by a group velocity tomographic study in the Scotia Sea region in order to minimize the non-uniqueness problem that results from the velocity-depth trade-off. The high noise level, typical of the oceanic environment, is overcome by stacking teleseisms with common receiver-station azimuthal angle and distance, and by selecting events with $m_b > 6.0$ within a range of distances between 30° to 85° . S-wave velocity models found beneath ESPZ and PMSA stations have a common velocity profile characterized by a large velocity gradient zone in the upper crust and by a smaller velocity gradient from the lower crust to the upper mantle. The depth of the crust-mantle transition zone beneath ESPZ and PMSA is about 37 km and 40 km, respectively.

INTRODUCTION

The Pacific margin of the Antarctic Peninsula (AP) is characterised by a complex structural framework (Barker, 1982; Larter & Barker, 1991). Its northern part shows transverse megafractures that represent the continuation of the oceanic fractures, involve the outcrop of the

basement and control the distribution of volcanic provinces on land (Hawkes, 1981). Two major oceanic fracture zones, the Hero and Shackleton fracture zones (HFZ and SFZ) (Fig. 1), form the boundary of the part of the Former Phoenix Plate where the spreading center has not been yet subducted, although it stopped the activity about 4Ma ago. The HFZ separates two different tectonic provinces; one

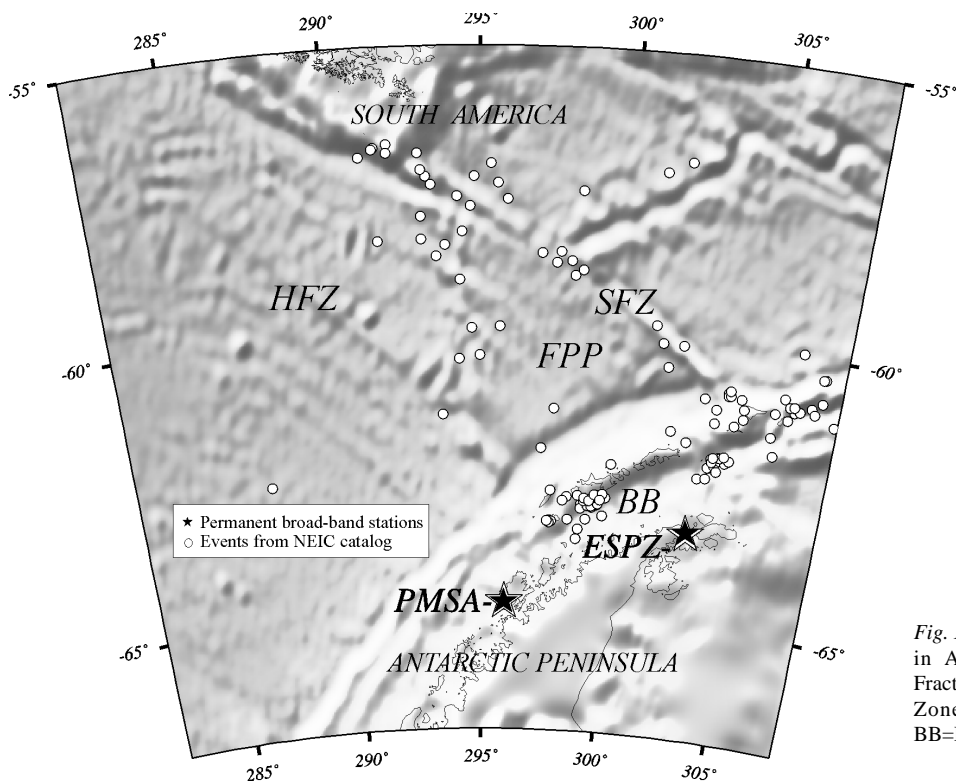


Fig. 1 - PMSA and ESPZ station locations in Antarctic Peninsula, (HFZ=Hero Fracture Zone; SFZ=Shackleton Fracture Zone; FPP=Former Phoenix Plate; BB=Bransfield Basin).

characterized by recent tectonic changes, north of the HFZ, while the second exhibits a low seismicity rate (Fig. 1). Northeast of the HFZ, the tectonic setting of the South Shetland margin is characterized by subduction of the Former Phoenix plate at the South Shetland Trench (SST). The Phoenix oceanic ridge is identified by the symmetry of marine magnetic anomalies across its axis (the youngest anomaly is 4.5 Ma old, Larter & Barker, 1991). The South Shetland Trench between the HFZ and SFZ, is characterized by normal faulting in sediments and basement on the oceanic side and folding and reverse faulting of the sediments on the landward side.

Southwest of the HFZ, subduction stopped after collision between the segments of the Aluk ridge and the trench. These segments were separated by fracture zones almost perpendicular to the margin that now divide sections of oceanic crust characterized by magnetic anomalies that become younger towards the continent (Herron & Tucholke, 1976; Barker, 1982).

The composite section across the AP (Tectonic map of the Scotia arc, 1985) shows that the cordillera has been uplifted by the magmatic arc intrusions. The predominant outcrops are accretionary prism sequences, with abundant intrusives and few remnants of volcanic rocks (Hole et al., 1991; Elliot et al., 1992).

A significant amount of single and multichannel seismic reflection surveys have been carried out across or adjacent to the continental margins of the AP in the last two decades (Cunningham et al., 1994). These data do not image deep crustal structures. A coarse information about the structure of the lithosphere in this region results from gravity and magnetic surveys (Renner et al., 1985; Parra et al., 1988; Garrett, 1991; Gonzales-Ferran, 1991). No other geophysical data, in relation with the deep crustal structure of AP are available.

Early refraction work was performed by Ashcroft (1972) in the South Shetland-Bransfield Strait area, indicating that the crust in the central Bransfield basin (BB) is probably oceanic, with a thickness less than 15 km, underlain by a mantle with a low seismic velocity (7.6-7.7 km/s). These results and other seismic investigations and geophysical studies (Henriet et al., 1992) combined with existing seismic data, suggested that the Bransfield Strait is floored by a rifted continental crust with spreading along the central volcanic area. Deep seismic refraction measurements (Guterch et al., 1985; Guterch et al., 1991a; Guterch et al., 1991b; Grad et al., 1993) did not provide a solution about the nature of the crust and two different hypothesis are still suggested: thin oceanic crust characterized by incipient sea floor spreading in opposition to a thicker anomalous crust, presently undergoing rifting. A recent group velocity tomography of the Scotia Sea region (Vuan et al., 2000) from the inversion of locally smoothed dispersion curves suggests that crustal shear wave velocities beneath the Bransfield Strait are typically continental with an average Moho depth of 25 km.

The crustal root of the AP is at present poorly defined and it seems, due to the thickness of the crust, no slabs of subducted material can be imaged by seismic refraction experiments. In this paper, we apply receiver function

inversion (*e.g.* Burdick & Langston, 1977; Vinnik, 1977, Owens et al., 1984; Ammon et al., 1990) on two permanent broad band seismic stations, deployed at the extreme tip of the AP (ESPZ) and southwest of the HFZ at Palmer station (PMSA), to retrieve the related crustal and upper mantle S-wave velocity models. The inversion is constrained by local group velocity dispersion curves derived from surface wave tomography.

EXTANT S-WAVE VELOCITY MODELS BENEATH ESPZ AND PMSA STATIONS

Crustal and upper mantle average S-wave velocity models beneath ESPZ and PMSA stations are represented by (1) local models obtained from the inversion of regionalized group velocity dispersion curves (Fig. 2; Vuan et al., 2000) and by (2) models extracted from a compilation of seismic refraction studies published in the period 1948-1995 (CRUST 5.1 model; Mooney et al., 1998). As shown in figure 2a similar dispersion curves are observed at ESPZ and PMSA stations from group velocity tomography. Although the spatial resolution of the geological and tectonic features by the two methods is different we observed a good agreement in averaging

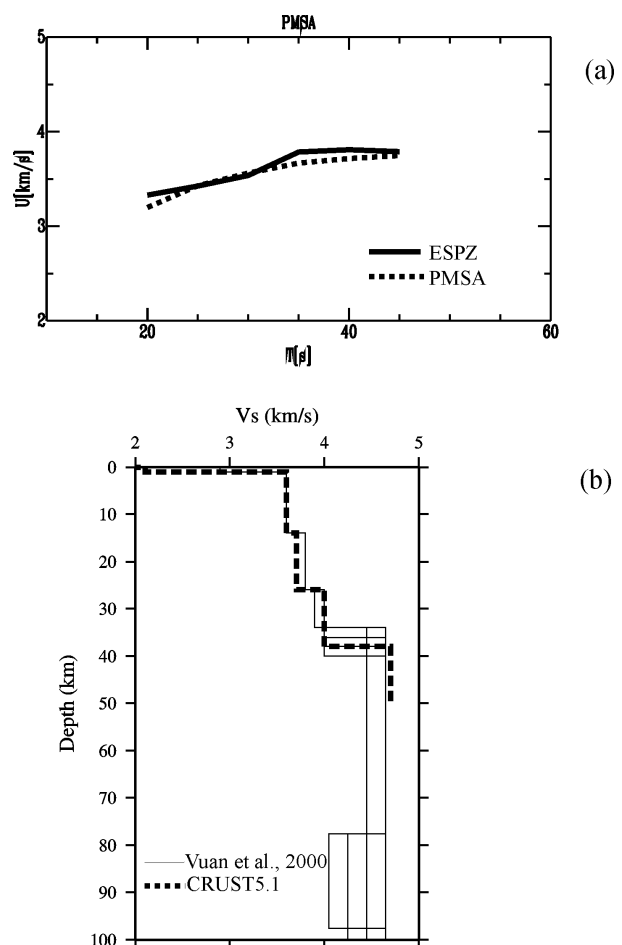


Fig. 2 - (a) Smoothed local group velocity curves at station sites derived from group velocity tomography (Vuan et al., 2000). (b) S-wave velocity models obtained from the inversion of the curves of figure 2a, overlaid to CRUST5.1 model (Mooney et al., 1998).

crustal S-wave velocities and the depth of the crust-upper mantle boundary (Fig. 2b). The average S-wave velocity of the crust ranges between 3.6 km/s (upper crust) and 4.0 km/s (lower crust) while the Moho is about 35 km to 40 km deep. Upper mantle S-wave velocity ranges from 4.5 km/s to 4.7 km/s. These models are quite similar to those found for the southernmost part of South America and are typical of stable continental regions (Vuan et al., 2000).

Smoothed group velocities obtained from the regionalization of the dispersion properties at ESPZ and PMSA locations (Fig. 2a) are used here to constrain the receiver function waveform inversion.

TELESEISMIC BODY WAVES

We selected a database of 350 teleseismic events with magnitude greater than 6. Preliminary processing revealed that 80% of the data were not suitable for a further analysis because of the high noise level. Furthermore the thick and fast average crust of AP, producing highly attenuated weak Pn arrivals, probably contributes to reject a large part of the data. The receiver function, described by Langston (1979), is formed from the spectral ratio of radial (or transverse) and vertical components from teleseismic P waves recorded at a single station. The functions obtained in this way are assumed to be free of source, mantle propagation and instrument response effects. The deconvolution is performed in the frequency domain (Owens et al., 1984) using a Gaussian filter width of 2.5 and trough filler value of 0.01.

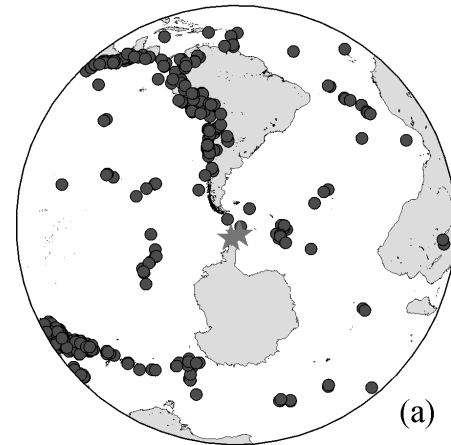
As shown in figure 3 seventy events are clustered mainly in two backazimuths (BAZ): northwest (epicentral distances from 60 to 85) and southeast (epicentral distances from 65 to 80). Receiver functions are stacked to improve the signal to noise ratio in the data. Radial and transverse components are shown in figure 4 for ESPZ and PMSA stations. Wave shape details and phase timing are distinct for different BAZ while at common BAZ the receiver function waveforms for the two stations are similar. On other BAZ quadrants (NE, SW) no sufficient amount of data is available to make possible the stacking procedure.

The transverse-component energy is a measure of the deviation from isotropic and planar structure (Ammon & Zandt, 1993). Normally the transverse-component of receiver function arrivals are characterized by a complex near surface scattering in the upper crust which cannot be modeled in any simple way (Langston, 1979). Therefore taking into account the better signal to noise ratio (see Fig. 4) we decide to invert only radial receiver functions.

INVERSION OF RECEIVER FUNCTIONS AND GROUP VELOCITIES

Receiver function analysis reveals the presence of S-wave velocity discontinuities at depth, but the absolute velocities and depths of the boundaries are not well resolved, as shown by the fit to the data provided by a suite of models (Ammon et al., 1990). Independent determination

dataset 350 events M >6.0



selected 70 events

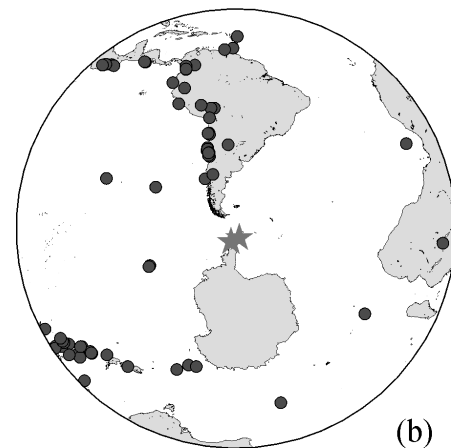


Fig. 3 - (a) The database of events before processing for receiver function analysis. (b) Resulting database after rejection of noisy records.

of the average crustal velocities (*e.g.* deep seismic soundings, surface wave dispersion data) can provide a better constrained model. We try to obtain S-wave velocity models beneath ESPZ and PMSA able to fit both P-S conversions observed on receiver functions and group velocity curves derived from our tomographic study (Vuan et al., 2000). We modified the Ammon et al., (1990) method that consists of a linearized iterative, least squares waveform fitting to include surface wave group or phase velocity constraints. Solutions must satisfy both receiver function waveforms and group velocity dispersion curves. To compute modeled receiver functions for a given velocity structure, a technique based on propagator matrix method is used (Kennet, 1983; Muller, 1985).

Previous published papers used a joint inversion of phase velocity data with receiver function waveforms (Ozalaybey et al., 1997; Du & Foulger, 1999). We used the same inversion method proposed by Du & Foulger, (1999) computing the partial derivatives of the group velocity with respect to model parameters and the theoretical dispersion curves with the algorithms developed by

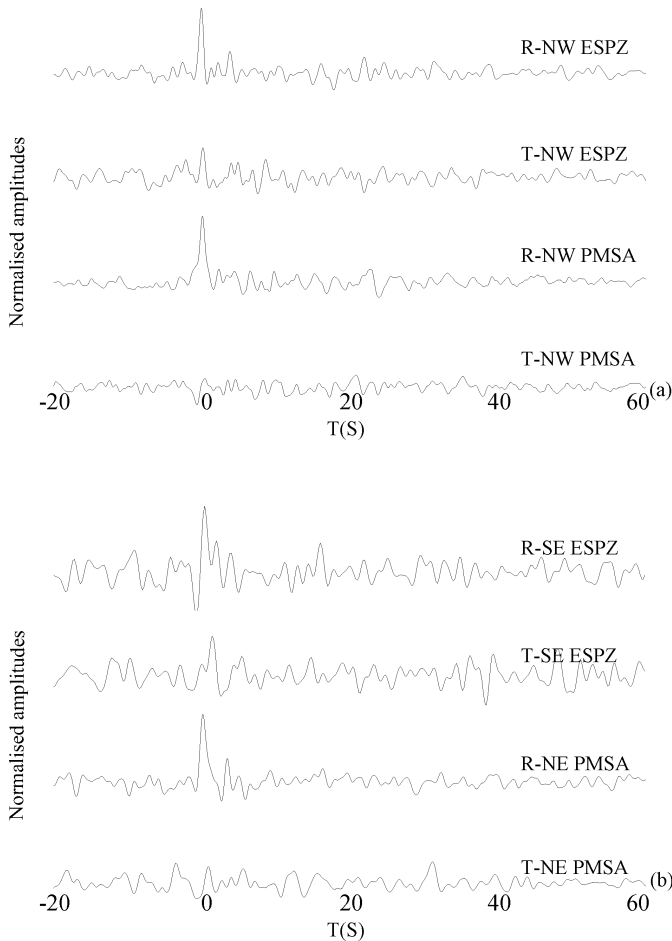


Fig. 4 - Examples of radial and transverse receiver functions observed for PMSA and ESPZ station at NW, SE and NE BAZ. To the upper right part of all the receiver functions the component (R=radial, T=transverse), the BAZ and the station are shown. Amplitudes of radial components are considerably larger than amplitudes of transverse components.

Herrmann (1987). *S*-wave velocity represents the independent parameter in our inversion while *P*-wave velocity and density were set assuming respectively a Poisson's ratio of 0.25 and the relationship $\rho = 0.32V_p + 0.77$ (Berteussen, 1977).

We choose as initial model the CRUST5.1 model (Mooney et al., 1998) for the tip of AP, able to satisfy well the local group velocity curves for ESPZ and PMSA. We split it with thin layers, 1 km thick for the first 14 km, and 2 km thick for intermediate layers until a depth of 40 km, and from this initial model we generate 32 different initial models with a cubic perturbation of 0.75 km/s and 15% of random component. A half space was placed below 60 km. We performed inversions for each perturbed initial model to find joint models that fit both receiver functions and group velocity data. We identify the Moho when *S*-wave velocity exceeds 4.5 km/s. NW BAZ stacked receiver functions are inverted both for PMSA and ESPZ stations. We inverted also receiver functions calculated at different BAZ quadrants (NE for PMSA, SE for ESPZ) to which the stacking procedure was not applied. This is done mainly to check the ability of the joint inversion to find solutions able to fit accurate group velocity measurements together with low quality receiver functions.

RESULTS

Figures 5 and 6 summarize the results obtained in the joint inversion of receiver function waveforms and group velocity dispersion curves beneath ESPZ and PMSA stations. We show only the smoothest solution of the *V_s* profile able to fit the observations. ESPZ receiver functions from NW and SE BAZ are selected and inverted together with the group velocity. NW receiver functions are simpler than the SE one and display almost the same arrivals for slightly different BAZ and epicentral distances. The velocity models (Fig. 5a) found are able to fit both the receiver function and observed group velocity (Fig. 5b, Fig. 5d). The main features of the NW BAZ *V_s* model are (1) a sharp velocity increase in the upper 10 km (2 km/s to 3.5 km/s), (2) a gradational crust-mantle transition zone with an upper mantle velocity value reached at about 35-37 km. The poor quality SE BAZ receiver function (Fig. 5c) is also inverted showing large differences from NW BAZ solutions in the uppermost 5 km. The upper crust is unconstrained by surface wave observations. Partial derivatives of group velocity with respect of *S*-wave velocity at 20 s are unable to constrain the upper 5 km.

Results from PMSA (Fig. 6) can be discussed mainly for NW BAZ where receiver function is better defined with tighter standard deviation bounds than NE receiver function. The features observed for ESPZ NW BAZ velocity model are repeated here for PMSA NW BAZ: a sharp increase in the *S*-wave velocity in the upper 10 km and (2) a gradational crust-mantle transition zone with upper mantle velocity reached at 40 km. On receiver function waveform we observe a broad Moho *P_s* phase clearly seen arriving at nearly 5s (Fig. 6b) implying a slightly thicker crust at this station. The NE BAZ receiver function (Fig. 6c), poorly defined by our data set, is here inverted too. It gives as result a faster velocity profile with similar large and small velocity gradients for respectively the upper crust and the lower crust-upper mantle.

CONCLUSIONS

The locally smoothed dispersion curves obtained from the regionalization of the group velocity measurements can be used to constrain better the receiver function inversion. The shear wave velocity models derived from group velocity tomography are able to explain only partially *P*-*S* conversions observed in receiver function waveforms at station locations.

A joint inversion able to satisfy both surface wave data and *P*-*S* conversions beneath station sites can represent a way to overcome the non-uniqueness problems related to receiver function waveform inversion (Ozalaybey et al., 1997; Du & Foulger, 1999).

Results obtained for the *S*-wave velocity models beneath PMSA are close to the two gradient profile (large velocity gradient in the upper crust and small velocity

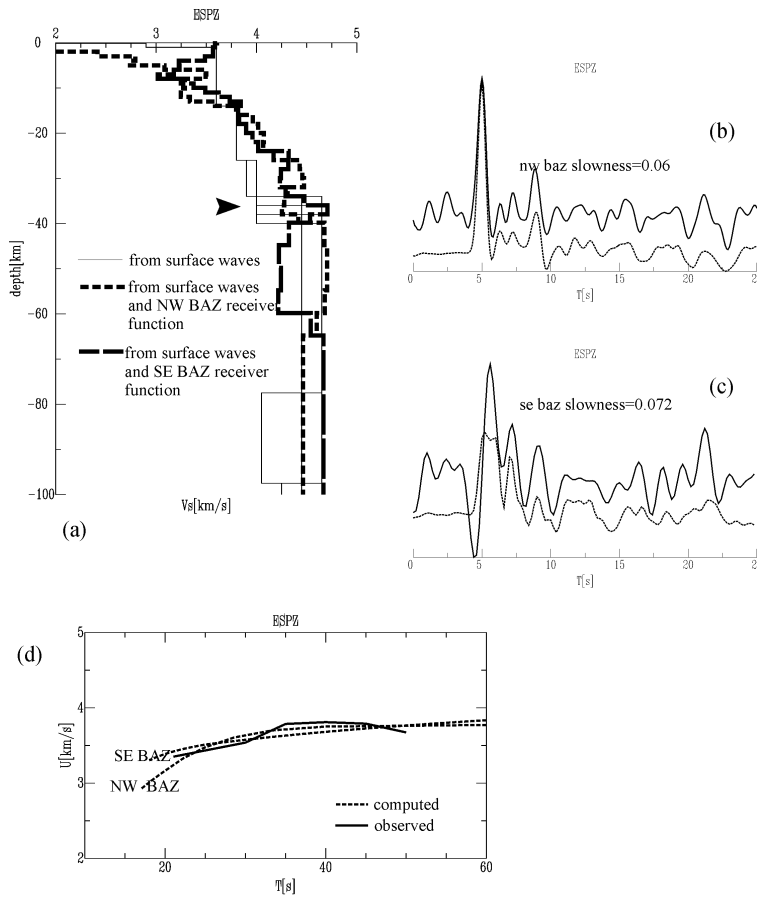


Fig. 5 - (a) S-wave smoothest velocity models beneath ESPZ obtained from the joint inversion. (b) NW BAZ observation (solid line) compared with the synthetic waveform computed using the model of figure 5a (dashed line). (c) SE BAZ observation (solid line) compared with the synthetic waveform computed using the model of figure 5a (dashed line). (d) Observed group velocity and calculated from the models of figure 5a.

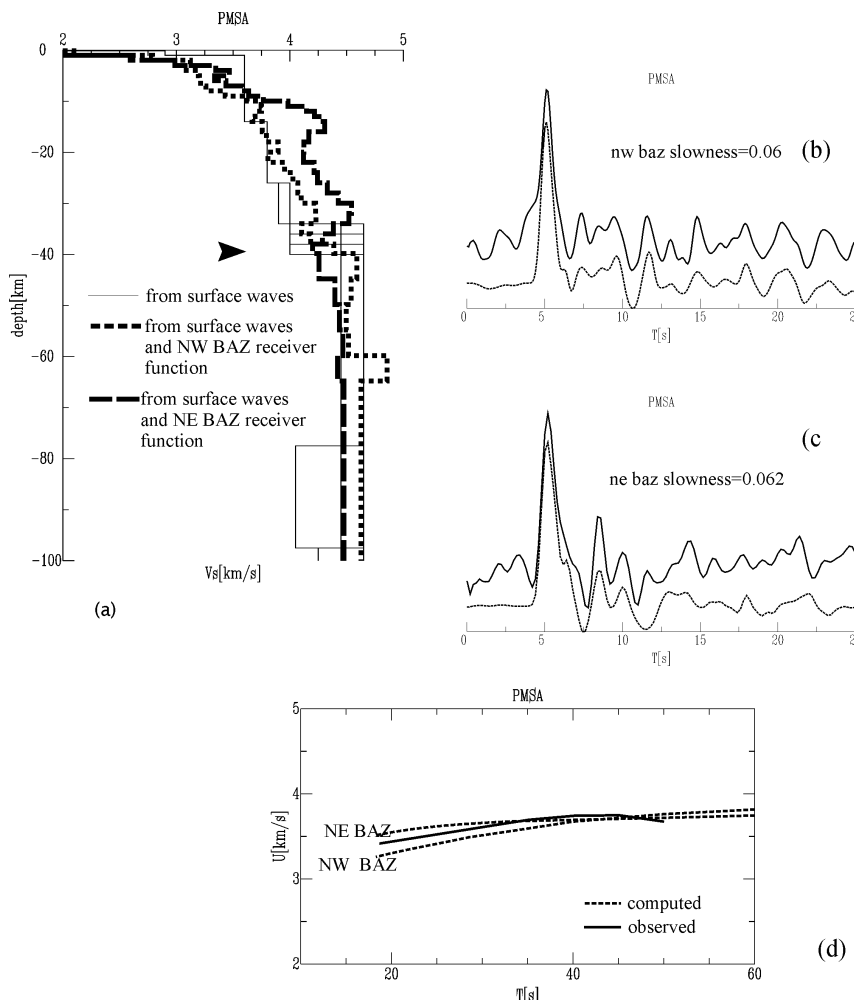


Fig. 6 - (a) S-wave smoothest velocity models beneath PMSA obtained from the joint inversion. (b) NW BAZ observation compared (solid line) with the synthetic waveform computed using the model of figure 6a. (c) NE BAZ observation compared (solid line) with the synthetic waveform computed using the model of figure 6a (dashed line). (d) Observed group velocity and calculated from the models of figure 6a (dashed line).

gradient from the lower crust to the upper mantle) found beneath ESPZ. The Moho discontinuity is deeper beneath PMSA than beneath ESPZ (~40 km vs. ~37 km). Some differences are observed on the upper crustal S-wave velocities. Middle and lower crust beneath PMSA is slightly faster than beneath ESPZ station. Results are preliminary and are mainly based on observations on NW BAZ.

Because of the high microseismic noise at the stations, a larger database, including receiver functions on all BAZ over a wide range of epicentral distances, is needed to confirm our models.

ACKNOWLEDGMENTS - This research has been funded by *Programma Nazionale di Ricerche in Antartide* (PNRA), projects 1B and 3A: *Struttura ed evoluzione dei Bacini Periantartici e dei Margini della Placca Antartica, Osservatori Geofisici e Geodetici*. An acknowledgement goes to the *Istituto Antartico Argentino* and *Istituto Nazionale di Oceanografia e Geofisica Sperimentale di Trieste* for the efforts made in the management and data acquisition of the Antarctic stations and to the IRIS consortium to have provided us data from PMSA station. We thank C.J. Ammon for making available to us the receiver function code and two anonymous referees for their useful suggestions. The public domain GMT graphics software (Wessel & Smith, 1991) has been used throughout.

REFERENCES

- Ammon C.J., Randall G.E. & G. Zandt 1990. On the nonuniqueness of receiver function inversions. *Journal of Geophys. Res.*, **95**, B10, 15303-15318.
- Ammon, C.J. & Zandt, G., 1993. Receiver structure beneath the southern Mojave block, California. *Bull. Seismol. Soc. Am.*, **83**, 737-755.
- Ashcroft, W.A., Crustal structure of the South Shetland Islands and Bransfield Strait. *British Antarctic Survey, Scientific Report* **66**, 1-43, 1972.
- Barker P.F., 1982. The Cenozoic subduction history of the Pacific margins of the Antarctic Peninsula: ridge crest-trench interactions. *Journal Geol. Soc. London*, **139**, 787-801.
- Berteussen K.A., 1977. Moho depth determinations based on spectral ratio analysis of NORSAR long-period P waves. *Phys. Earth Planet. Inter.*, **31**, 313-326.
- Burdick I. J. & Langston C.A., 1977. Modeling crustal-structure through the use of converted phases in teleseismic body-waveforms. *Bull. Seismol. Soc. Am.*, **67**, 677-691.
- Cassidy J.F., 1992. Numerical experiments in broadband receiver function analysis. *Bull. Seism. Soc. Am.*, **82**, 1453-1474.
- Cunningham A.P., Vanneste L.E. & the ANTOSTRAT Group, 1994. The ANTOSTRAT Antarctic Peninsula Regional Working Group digital Navigation Compilation, *Terra Antartica*, 1(2), 265-266.
- DuZ.J. & Foulger G.R., 1999. The crustal structure beneath the northwest fjords, Iceland, from receiver functions and surface waves. *Geophysical Journal International*, in press.
- Elliot D.H., Hoffman S.M. & Rieseke D.E., 1992. Provenance of Paleocene strata, Seymour Island. In: Y. Yoshida, K. Kaminuma & K. Shiraishi (eds.), *Recent Progress in Antarctic Earth Sciences*, TERRAPUB, Tokyo, 347-355.
- Garrett S.W., 1991. Aeromagnetic studies of crustal blocks and basins in West Antarctica: a review. In: M.R.A. Thomson, J.A. Crame & J.W. Thomson (eds.), *Geological evolution of Antarctica*, Cambridge, Cambridge University Press, 251-256.
- Grad M., Guterch A. & T. Janik, 1993. Seismic structure of the lithosphere across the zone of subducted Drake plate under the Antarctic plate, West Antarctica. *Geophysical Journal Int.*, **115**, 586-600.
- Guterch A., Grad M., Janik T., Perchuc E. & Pajchel J., 1985. Seismic studies of the crustal structure in west Antarctica 1979-1980 — preliminary results, *Tectonophysics*, **114**, 411-429.
- Guterch A., Grad M., Janik T. & Perchuc E., 1991a. Tectonophysical models of the crust between the Antarctic Peninsula and the South Shetland Trench. In: M.R.A. Thomson, J.A. Crame & J.W. Thomson (eds.), *Geological evolution of Antarctica*, Cambridge, Cambridge University Press, 499-504.
- Guterch A., Shimamura H. & the Polish-Japan-Argentina Research Group, 1991b. An OBS land refraction seismological experiment in the Bransfield trough, west Antarctica, 1990/91. *Abstracts of the sixth Int. Symposium on Antarctic Earth Sciences*, NIRP, Tokyo, 201-202.
- Gonzales-Ferran O., 1991. The Bransfield rift and its active volcanism, In: M.R.A. Thomson, J.A. Crame & J.W. Thomson (eds.), *Geological Evolution of Antarctica*, Cambridge University Press, New York, 505-509.
- Hawkes D.D., 1981. Tectonic segmentation of the Northern Antarctic Peninsula. *Geology*, **9**, 220-224.
- Henriet J.P., Meissner R., Miller H. & the GRAPE Team, 1992. Active margin processes along the Antarctic Peninsula. *Tectonophysics*, **201**, 229-253.
- Herron E.M. & Tucholke B.E., 1976. Sea-floor magnetic patterns and basement structure in the southeastern Pacific, *Initial Rep. Deep Sea Drilling Project*, **35**, 263-278.
- Herrmann R.B., 1987. *Computer Programs in Seismology*, Vol. IV. Surface wave inversion, Saint Louis University.
- Hole M.J., Pankhurst R.J. & Saunders A.D., 1991. Geochemical evolution of the Antarctic Peninsula magmatic arc: the importance of mantle-crust interactions during granitoid genesis. In: M.R.A. Thomson, J.A. Crame & J.W. Thomson (eds.), *Geological evolution of Antarctica*, Cambridge, Cambridge University Press, 369-374.
- Kennett B.L.N., 1983. *Seismic wave propagation in stratified media*, Cambridge University Press, New York.
- Langston C.A., 1979. Structure under Mount Rainier, Washington, inferred from teleseismic body waves. *J. Geophys. Res.*, **84**, 4749-4762.
- Larter R.D. & Barker P.F., 1991. Effects of ridge crest-trench interactions on Antarctic-Phoenix spreading: forces on a young subducting plate. *Journal of Geophysical Res.*, **96**, 19583-19607.
- Mooney W.D., Laske G. & Masters G., 1998. CRUST5.1: A global crustal model at 5 degrees by 5 degrees. *Journal of Geophysical Res.*, **103**, 727-747.
- Muller G., 1985. The reflectivity method: a tutorial. *Journal of Geophysics*, **58**, 153-174.
- Owens T.J., Zandt G. & Taylor S.R., 1984. Seismic evidence for an ancient rift beneath the Cumberland Plateau, Tennessee: A detailed analysis of broadband teleseismic P waveforms. *Journal of Geophysical Res.*, **89**, 7783-7795.
- Ozalaybey S., Savage M.K., Sheehan A.F., Louie J.N. & J.N. Brune, 1997. Shear-wave velocity structure in the northern Basin and Range Province from the combined analysis of receiver functions and surface waves. *Bull. Seism. Soc. Am.*, **8**(1), 183-199.
- Parra J. C., Yanez G. & Grupo de Trabajo USAC, 1988. Aeromagnetic survey on the Antarctic Peninsula and surrounding seas: integration of the data obtained at different altitudes, Serie Cientifica del Instituto Antartico Chileno, 38, 117-131.
- Renner, R.G.B., Sturgeon, L.J.S. and Garrett, S.W., Reconnaissance gravity aeromagnetic surveys of the Antarctic Peninsula, B.A.S. Scientific Reports, **110**, Cambridge, 1985.
- Tectonic Map of the Scotia Arc, 1985. 1:3000000, British Antarctic Survey, Cambridge.
- Saul J., 1997. InVRF: A package for the computation and inversion of teleseismic receiver functions, V. 1.2.4., Institute of Geophysics, University of Hamburg, Germany.
- Vinnick L.P., 1977. Detection of waves converted from P to SV in the mantle. *Phys. Earth Planet. Inter.*, **15**, 39-45.
- Vuan A., Russi M. & Panza G.F., 2000. Group velocity tomography of the sub-antarctic Scotia Sea region. *Pure and Applied Geophysics*, **157**, 1337-1357.